Journal of Hazardous Materials, 34 (1993) 313–333
Elsevier Science Publishers B.V., Amsterdam

Stochastic modeling of flow and transport in deep-well injection disposal systems

Seung-Whee Rhee[a,*], Danny D. Reible[a] and W. David Constant[b]

[a]*Department of Chemical Engineering, Louisiana State University, Baton Rouge, LA 70803 (USA)*
[b]*Hazardous Waste Research Center, Louisiana State University, Baton Rouge, LA 70803 (USA)*

(Received July 15, 1992; accepted in revised form December 24, 1992)

Abstract

The migration of deep-well injected waste in heterogeneous confining layers is evaluated using numerical simulation. Of primary concern is the migration potential through permeable sand paths between less permeable shale. The configuration of the predominantly shale confining layers was defined by Monte Carlo techniques assuming a binary random structure composed of pure sand and pure shale. Three-dimensional flow simulations using MODFLOW, a finite difference model, indicated that essentially continuous sand paths and unacceptably rapid transport might exist through confining layers with an average shale fractions of less than about 0.65 and that two and three dimensional flow simulations were essentially equivalent for high (>0.6–0.7) or low (<0.4–0.5) shale fractions. Diffusion and advection–dispersion in the configurations with a shale fraction greater than 0.65 were estimated via a two-dimensional finite element model. Interaction between organic constituents of the waste and the soil media is represented by linear sorption. The model was applied to an example in which dilute aqueous solutions of acrylonitrile were deep-well injected. Advective penetration of a representative confining layer over 10,000 years was found to be small (<3 m assuming injection pressures were maintained throughout the period). Even including diffusion and dispersion, concentrations in excess of drinking water criteria did not extend beyond the confining layers after simulation for 10,000 years.

Introduction

Disposal of liquid hazardous waste by subsurface injection has come into favor as a means of waste disposal because of its relatively low cost. In 1981, about 60 percent of all hazardous wastes in the U.S. were disposed of by deep-well injection [1]. Most injected wastes are mineral acids or water contaminated by small amount of hazardous materials. The wastes are injected into relatively permeable formations confined by adjacent low permeability

*To whom correspondence should be addressed.

0304-3894/93/$06.00

shales. As increasing volumes of hazardous materials have been injected into the subsurface, concern for contamination of underground sources of drinking water has grown. Much of the concern regarding deep-well injection arises from the lack of information available on the transport and ultimate fate of hazardous materials after injection.

The Resource Conservation and Recovery Act of 1976 (RCRA, U.S. Public Law 94-580) suggested that all deep-well injection projects be banned by August 1988 unless they were shown to be protective of human health and the environment. The U.S. Environmental Protection Agency (EPA) proposed that hazardous waste disposal by deep-well injection be banned unless it can be shown that the injected waste will be rendered non-hazardous in the disposal zone or that the waste will remain confined for at least 10,000 years [2].

Modeling is required to predict underground waste movement and the ultimate fate of the waste over this time period. Due to uncertainties in the subsurface fate processes, most efforts in support of petitions for deep-well injection have focused on demonstrating negligible migration through the confining layers. In general, such petitions have assumed that the shale confining layers are essentially homogeneous, low permeability strata and that diffusion is the most important migration mechanism. In the present work, the effect of heterogeneities in the sand shale system will be considered. In particular, the effect of high permeability sand inclusions on the waste migration potential will be evaluated through numerical simulation of flow and transport in stochastically generated representations of the confining layer structure.

Fogg [3] discussed the topic of sand-body interconnectedness in the Wilcox aquifer system, Texas. He found that the channel-fill sand bodies appeared to be laterally interconnected where sand percent exceeded 20% and disconnected where sand percent was less than 20%. Even though there were virtually no data on the vertical interconnection of sand-body, anisotropy ratio of hydraulic conductivity was reasonably 10^{-4}. Hence, it could be expected that vertical interconnection in sand bodies be much more difficult than lateral interconnection.

Since most natural subsurface formations display a significant variation in permeability due to heterogeneity, considerable effort has been devoted to the problem of estimating the effective permeability when the local permeability is spatially variable. Two main stochastic approaches are available for estimating effective permeabilities in heterogeneous porous media: numerical methods based on Monte Carlo simulations [4–7] and analytical methods based on perturbation theory [8–10]. While the most desirable estimate of subsurface flow is obtained using an analytical solution, a spectral analysis method based on small perturbations in permeability is inappropriate for the assessment of problems in which the input variables have a large variance.

Several researchers [7, 9, 11] found that the most probable behavior of a heterogeneous system approaches that of a homogeneous system with an effective permeability expressed by the geometric mean of the individual permeabilities. Desbarats [12] numerically estimated effective permeabilities in a sand–shale

formation under steady state uniform flow conditions. His simulations were limited to a sand–shale permeability ratio of 10^4 to 1, although this ratio is of the order of 10^7 to 1 in the region of interest here. He found that the effective permeability was a function of the shale volume fraction, the spatial correlation structure, and the flow field dimensionality. For the case of binary permeability distribution and an isotropic formation, Desbarats' numerical results were found to agree fairly well with a self-consistent formula for effective permeability derived by Dagan [13]. Kramers et al. [14] used petrographic image analysis to characterize the structure of low shale fraction gas reservoir systems. They showed that the shale significantly reduces the permeability of these zones.

To estimate the effective horizontal and vertical permeability, Haldorsen and Lake [15] developed an analytical expression based on a stream tube concept for each grid block in the simplified flow field. The stream tube approach relates effective permeability to the tortuosity of flow paths through the medium. Begg et al. [16] revised this approach to get effective vertical permeability without generating a synthetic subsurface formation. Desbarats [12] suggested that the stream tube approach had reasonable results only at low shale fraction because the approach contained an implicit shale noninteraction assumption which was violated even at moderate shale fraction.

The estimation of flow or effective permeability in the above studies is limited to low shale fraction formations or low contrast between sand and shale permeability. These limitations are relaxed herein. In addition, since the primary quantity of interest is chemical transport of the injected wastes and not bulk flow, transport modeling is also addressed.

Dispersion in heterogeneous porous media occurs because of the spatial variability in the velocity field, which in turn, is primarily due to the variability in hydraulic conductivity. This spatial variability is explicitly modeled herein at a distance scale greater than or equal to the height of the shale zones. At smaller scales, Fickian dispersion is assumed. Scale dependent dispersion at smaller scales [11, 17] is not modeled but this effect has been suggested to be minimal at long times [18, 19]. Fickian models have also been used previously to model dispersion in heterogeneous media [10, 20–23]. Recently, for low shale fractions, it has been shown that macrodispersive transport in sand–shale sequences cannot be represented by Fickian models because of channeling [24].

The current approach uses a numerical simulation of the flow and transport in a Monte Carlo generated sand–shale formation. By generating large numbers of configurations, the statistics of the waste migration potential can be defined. The confinement zone was modeled as a combination of binary random structures composed of either pure sand or pure shale. The effective permeability of each hypothetical configuration was evaluated by solving the steady-state, incompressible ground-water flow equation via a finite element method. The expected value and 95% confidence limits for effective permeability in the actual subsurface configuration were assumed represented by the statistics of the ensemble of hypothetical configurations.

The penetration of wastes into the confining layer is obtained by solving the transient advection–dispersion equation for solute transport via a finite element method [14, 25]. In the solute transport equation, the velocity field from the flow modeling is used to solve the concentration profile. Because of the coupled nature of flow and transport equations, the transport simulations were limited to two-dimensional simulations in a particular subsurface configuration. The transport simulations were limited to high shale fractions, where the flow modeling suggested that the effective permeability was not sensitive to the particular subsurface configuration. From the concentrations predicted by the numerical simulations, concentration isopleths are generated within the hypothetical confining layers and mean concentration profiles are obtained as a function of shale fraction. Finally, the penetration distance of a weakly sorbing contaminant, acrylonitrile, was estimated.

Generation of subsurface formations

An empirical shale fraction profile as a function of depth in subsurface formations can be determined at a specified site from observed well log data using gamma ray and spontaneous potential–resistivity logs. The well log can also identify layers and layer thickness. The focus of this study is on the flow and transport through the shale confining layers that represent the primary resistance to migration of injected wastes. A confining layer is assumed to be composed of a random sequence of sand and shale in proportion to the average shale content of that layer as defined by well logs. Well log information is also used to estimate the thickness of a particular layer. Confining strata are assumed to exhibit no fractures and faults.

In order to generate the configuration of confining layers, statistics of shale thickness, shale width and shale fraction are needed. Since the lateral dimension of the shale regions remain unknown except for nearby wells, individual shale zone positions and their width are randomly selected from a distribution function under an assumption that each shale zone is independent of all other shale zones. For simplicity, the shale width distribution is assumed defined by a triangular distribution function which can be specified by a maximum, a minimum and a most probable value. Random placement of the shale zones within an initially sand-filled media is continued until the shale fraction in the layer reaches the level estimated by well log data. Overlapping shale zones are possible in the random placement algorithm and the shale fraction was corrected to avoid double-counting of this shale.

Haldorsen and Lake [15] suggested a similar approach that generated a configuration of 2D sand–shale formations with a specified fraction of shale using statistical techniques. In their work, the thickness and width of shale were sampled from an empirical cumulative distribution, while the position of shale was assigned randomly. It is necessary to employ a large number of elements to determine the configuration of the subsurface formation with their techniques.

In this study, we modify their technique to reduce the number of elements and to allow for lateral overlapping. The thickness of confining layers is inferred from the actual well log data while the thickness of shale is assumed to be uniform within a given confining layer. The position and width of shale are assigned randomly.

At low shale fractions, permeable sand veins are essentially continuous, allowing potentially rapid vertical transport. At high shale fractions, however, sand zones are isolated by shale regions so that transport paths through high permeability sand veins may not exist. As expected, the degree of lateral overlapping and the number of isolated sand zones increases as the shale fraction and the aspect ratio of the shale zones, defined by the ratio of width to thickness of shale zone, increase. The lateral dimensions (length and width) of sand or shale zones are typically much greater than their vertical dimension (thickness) [26]. The effective vertical permeability of a formation increases as the aspect ratio decreases [14, 27]. The effective horizontal permeability is almost independent of the aspect ratio [12, 27]. An aspect ratio of unity provides a reasonable upper bound to the effective vertical permeability.

Hypothetical confining strata for shale fractions of 0.66 and 0.88 are shown in Figs. 1 and 2, respectively, for the particular case of uniform thickness shale layers. In these configurations, white and dark spaces represent sand and shale

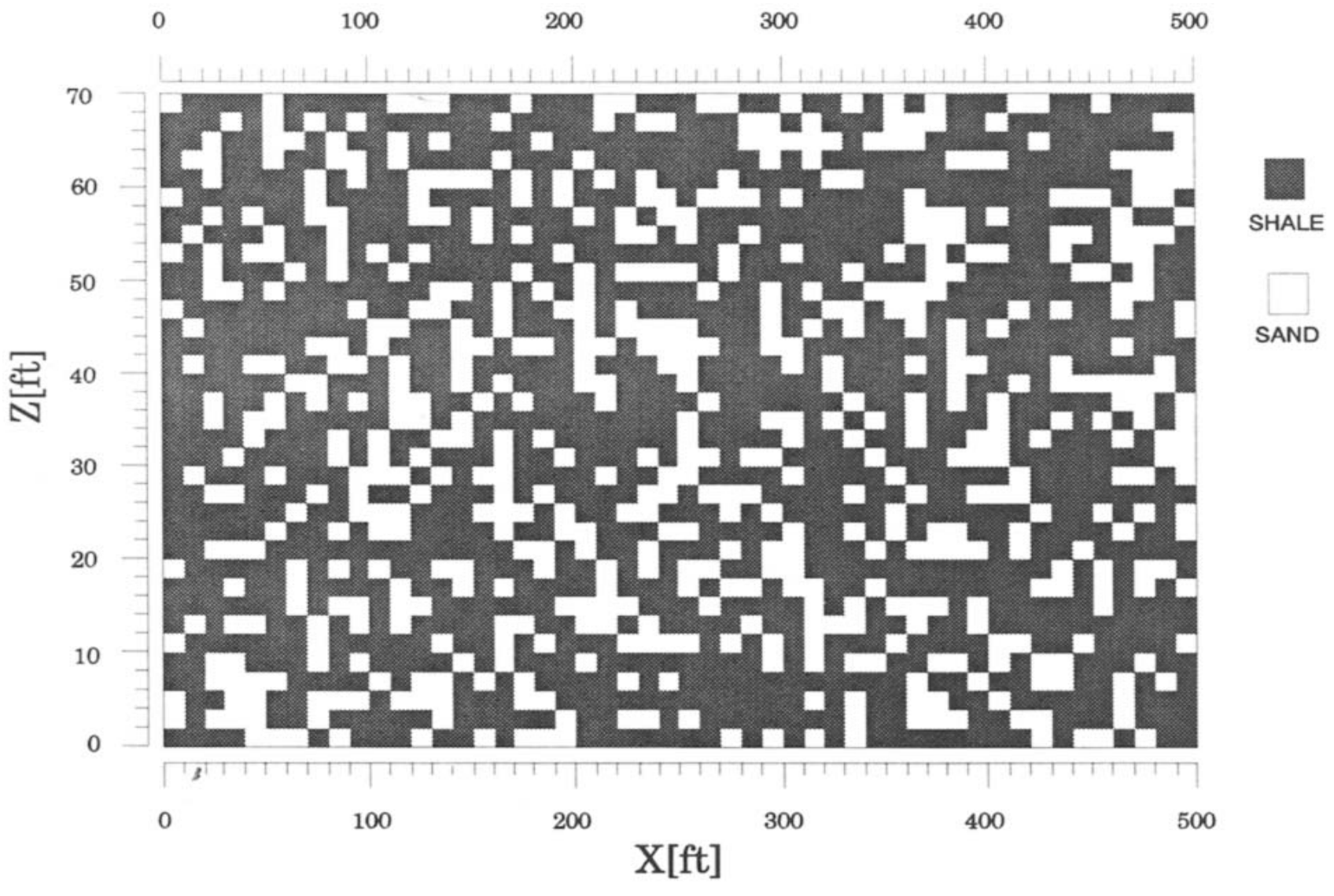

Fig. 1. Hypothetical confining strata at shale fraction 0.66. (Note that the vertical scale is exaggerated with respect to the horizontal scale.)

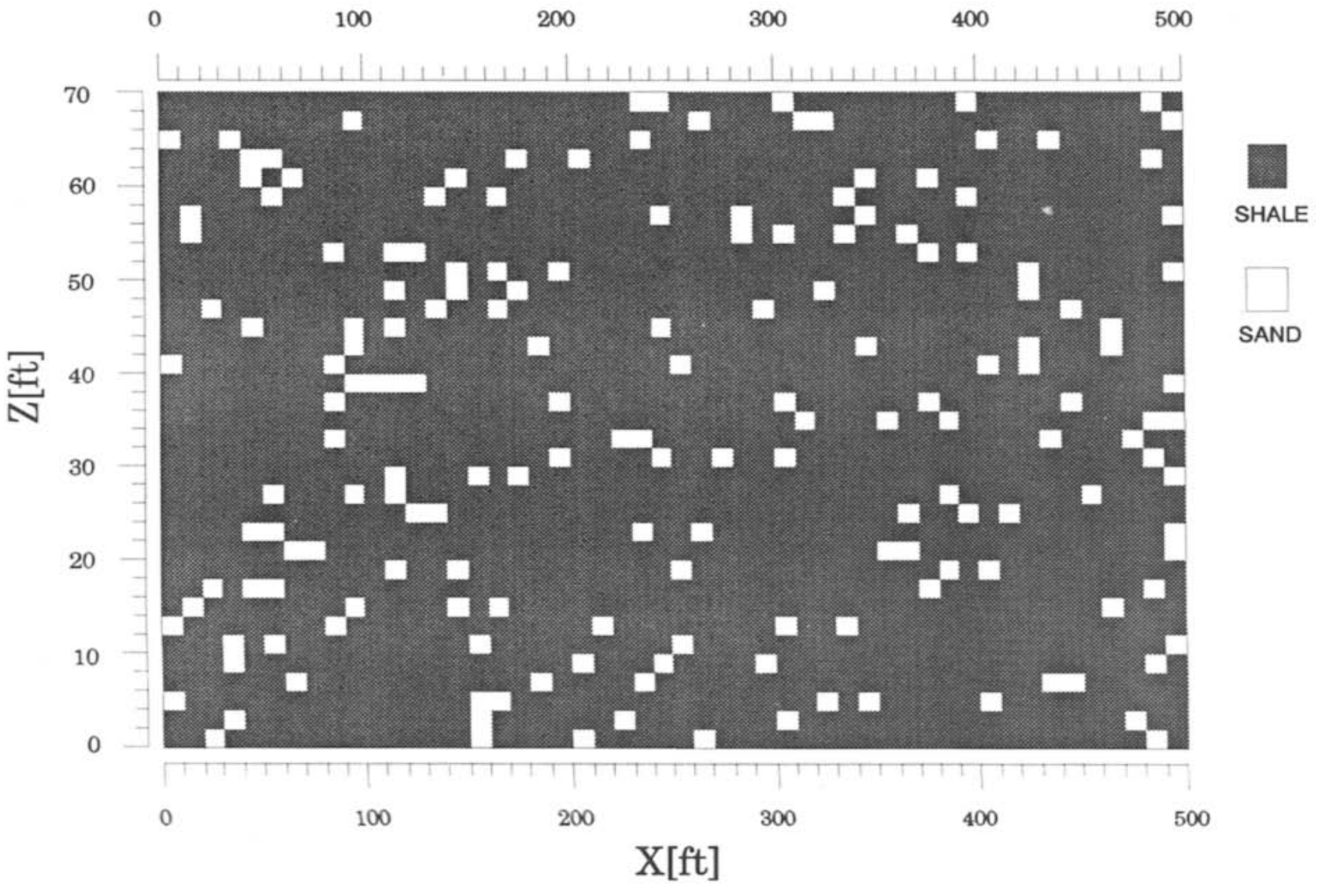

Fig. 2. Hypothetical confining strata at shale fraction 0.88. (Note that the vertical scale is exaggerated with respect to the horizontal scale.)

regions, respectively. These figures represent only a part of the configuration (i.e. 70 ft [21.34 m] of the total simulated confining layer depth of 300 ft (91.44 m). For all shale fractions greater than about 0.65, sand zones are isolated by shale regions.

For a 2D configuration of confining layers, the shales are continuous in the third dimension so that the flow may be blocked by continuous shales in that direction. If shales are not continuous in the third direction, the availability of permeable flow paths may increase. A preliminary 3D modeling effort was initiated to examine the potential for enhanced flow in a 3D system. The same principles as those utilized in the 2D descriptions were used to generate the configuration in the third-dimension. The 3D configuration is generated by combining each 2D independent configuration laterally. In the 3D configuration, the aspect ratio of width to thickness of shale zone was fixed at 1. The potential for continuous permeable sand veins and therefore a high vertical permeability is maximized with this aspect ratio.

Numerical simulation of flow in confining layers

Subsurface flow in confining layers depends mainly on the sand distribution because of the low permeability of shale. According to Freeze and Cherry [28],

the range of shale permeability is from 0.00001 mdarcy to 0.1 mdarcy. These shale permeabilities are typically several orders of magnitude lower than the intrinsic sand permeability. In this study, shale permeability is assumed to be of the order of 0.0001 mdarcy and sand permeability of order 1000 mdarcy a ratio of 10^7. This is the magnitude of the permeabilities measured by Constant and Clark [29] using samples of shale from disposal wells in Jefferson Parish, Louisiana. The modeled confining layer configuration of randomly placed sand and shale zones is extremely heterogeneous. A non-uniform finite element grid is used to perform the flow simulation in the heterogeneous porous media. Previous work by Desbarats [12] was limited to a sand–shale permeability ratio of 10^4.

The 3D steady-state subsurface flow in an incompressible saturated confining layer is governed by [28]:

$$\frac{\partial}{\partial x}\left(K_x \frac{\partial h}{\partial x}\right)+\frac{\partial}{\partial y}\left(K_y \frac{\partial h}{\partial y}\right)+\frac{\partial}{\partial z}\left(K_z \frac{\partial h}{\partial z}\right)=0, \tag{1}$$

where K_i represents hydraulic conductivity in ith direction and h is the hydraulic head. Constant head boundary conditions are specified in the mean (vertical) direction of flow, and no flow conditions are imposed on side boundaries.

The finite element method based on the Galerkin technique is used to formulate the model of the two-dimensional movement of hazardous wastes in confining layers. The numerical model utilizes linear triangular elements. Even though a Monte Carlo technique is applied to generate the confining layer configuration, any individual configuration is deterministic. The Monte Carlo technique is used to generate an ensemble of configurations, and the deterministic model is used to solve the flow problem for each configuration. The means and variances of the hydraulic head and effective permeability obtained from the set of deterministic solutions should indicate the expected value and uncertainty in these parameters in the real subsurface formation.

The flow calculation and determination of the effective permeability is repeated for each generated configuration of the confinement zone. Reduced effective vertical permeabilities for each configuration are defined by dividing the effective vertical permeabilities by sand permeability. To get the expected value of the effective vertical permeability of the confinement zone, the geometric mean permeability of up to 600 different configurations is used at the same shale fractions. If the expected value of effective vertical permeability is estimated by arithmetic mean, the expected value is extremely overestimated. After 300 configurations there is little change in the expected value of effective vertical permeability with the number of configurations. The 95% confidence limits are determined directly from the observed distribution of the calculated effective permeabilities.

Since the range of possible effective permeability may increase in higher dimensions, the three-dimensional flow problems were investigated by using the Finite Difference Method computer tool MODFLOW [30]. The flow system is discretized by a block-centered, and $30 \times 40 \times 30$ nodal grid. The flow equation, which is approximated by a standard seven-point finite difference scheme, is solved by using slice successive overrelaxation (SSOR).

Numerical simulation of solute transport

The general governing equation describing the two-dimensional solute transport in a saturated, essentially incompressible porous medium is [31]

$$R_f \frac{\partial C}{\partial t} + \frac{\partial}{\partial x}(v_x C) + \frac{\partial}{\partial z}(v_z C) = \frac{\partial}{\partial x}\left(D_x \frac{\partial C}{\partial x}\right) + \frac{\partial}{\partial z}\left(D_z \frac{\partial C}{\partial z}\right) \tag{2}$$

where C represents the constituent concentration in solution, R_f is retardation factor, t is time, v_i is the velocity in the ith direction, D_i is the hydrodynamic dispersion coefficient in the ith direction. Initial condition is zero concentration in the domain of confining strata. No flux boundary conditions are imposed in the x-direction and constant concentration boundary conditions were specified in the z-direction. Since the horizontal hydraulic head difference is much less than the vertical hydraulic head difference in the results of the flow simulations, horizontal advection is negligible under the conditions simulated.

The components of the dispersion tensor have contributions from both mechanical dispersion and molecular diffusion. The principal values of the dispersion tensor **D** are given by

$$D_x = \alpha_T v_z + D_{eff}, \tag{3a}$$

$$D_z = \alpha_L v_z + D_{eff}, \tag{3b}$$

where α_L is the longitudinal (vertical) dispersivity, α_T is the transverse (lateral) dispersivity, and D_{eff} is the effective diffusivity. The longitudinal dispersivity or dispersivity in the direction of travel usually scales with the characteristic size of the heterogeneities of the media.

For advection dominated transport (Peclet number, $Pe \approx v\Delta z/D_{eff} > 1$), a conventional finite element model is generally inappropriate. In this case, however, the maximum value of the Peclet number, which represented the ratio of advection to diffusion, varied from 0.33 to 0.85 as the shale fraction was decreased from 0.88 to 0.66. Since the Peclet number is of order of unity or less at these high shale fractions, the advection–diffusion model of solute transport is solved using the Galerkin finite element method with the distribution of real velocity fields obtained from the steady state flow equation. The Galerkin finite element calculation procedure employed for flow and transport equations is an

adaptation of that described by Smith and Griffiths [32]. A fully implicit backward difference scheme is employed for the time derivative.

The size of the hypothetical configuration of confining strata was 200 ft (60.96 m) in depth and 500 ft (152.4 m) in width. In the numerical simulation of flow and transport in the hypothetical formation, an irregular array of nodal points were assigned to conform to the complex geometry of the medium. Due to computational limitations, only a single generated configuration at each shale fraction was used in the transport modeling. At the high shale fractions used, however, flow modeling suggested that the effective permeability or average flow was insensitive to the particular subsurface configuration. The transport field was discretized by a 100×50 nodal grid. Numerical simulations were performed for four hypothetical configurations with 0.66, 0.7, 0.8 and 0.88 shale fraction over 10,000 years.

Recently, Neuman [33] investigated the universal scaling of dispersivities in geological media. He showed that the dispersivity data from laboratory and field tracer studies in porous and fractured media increased with the distance traveled. He suggested the following formulation for the universal dispersivity as a function of the characteristic length for travel distance, L_s:

$$\alpha = 0.017\, L_s^{1.5}, \tag{4}$$

where L_s is in meters. The formula is limited to $L_s < 100$ m. Maximum travel distances of contaminant concentrations within an order of magnitude of that at the injection point are of the order of 10–20 m. Equation (4) suggests a travel distance of 15 m corresponds to a dispersivity of about 1 m. This should be a reasonable upper bound for dispersivity in that the dispersion attributable to heterogeneities at the layer depth scale and larger is explicitly modeled. Only the subgrid scale should be modeled with an effective dispersion coefficient.

The effective diffusivity in the sand was estimated from the model of Millington and Quirk [34]. The effective diffusivity in the shale was as estimated by Berner [35]. The effective diffusivity for shale, corrected for tortuosity, assumed in this study is the same as that used by Ranganathan and Hanor [36]

$$D_{\text{eff}} = D_{\text{m}} \varepsilon^3 \tag{5}$$

and for sand [34]

$$D_{\text{eff}} = D_{\text{m}} \varepsilon^{1/3}, \tag{6}$$

where D_{m} is molecular diffusivity and ε is the porosity. For comparison, the diffusion controlled problem was also investigated by neglecting the advection term in the solute transport equation.

In eq. (2) it has been assumed that the chemical interaction of contaminant and subsurface soils is limited to linear, reversible sorption. If local linear

equilibrium is assumed, a retardation factor due to sorption can be defined as [28]

$$R_f = 1 + \rho_b K_d / \varepsilon, \tag{7}$$

where ρ_b is the bulk mass density of the porous medium, and K_d is the partition coefficient. The retardation factor, R_f, represents the velocity of the subsurface fluid relative to that of the primary constituent and results from the accumulation of contaminant in the immobile as well as mobile phase. For a partition coefficient that is orders of magnitude larger than unity, the solute is essentially immobile [28]. Since the sorption of hydrophobic compounds (e.g. aromatic hydrocarbons and chlorinated hydrocarbons) in sand is much smaller than that in silt and clay [37], sorption in sand regions is assumed to be negligible in these simulations ($R_f = 1$). The content of organic carbon in shale is typically less than 0.3%. For organic carbon contents greater than 0.1%, partitioning is typically dominated by organic carbon. Thus, an organic carbon based partition coefficient can be used to estimate sorption [38]. The partition coefficient for any given soil is the product of the organic carbon based partition coefficient K_{oc} and the weight fraction of organic carbon f_{oc} in the soil (i.e. $K_d = K_{oc} f_{oc}$). Among the compounds that have been observed as trace components of a particular deep-well injected waste are acrylonitrile ($K_{oc} = 0.85$), 1,2-dichloroethane (EDC, $K_{oc} = 14$), and methylmethacrylate ($K_{oc} = 840$) [39]. Assuming 0.3% (w/w) organic carbon, the partition coefficients of these compounds range from 0.0026 for acrylonitrile to 2.52 for methylmethacrylate. The range of the shale partition coefficient employed in the model was thus varied from 0 to 3 and the retardation factor from 1 to 17.7.

Acrylonitrile will be used here as an example for the purposes of estimating solute transport. A particular deep well injection stream contains acrylonitrile with a concentration of 760 mg/L while the drinking water standard is 5.8×10^{-5} mg/L. Hence, the required dilution ratio for which containment must be demonstrated over the 10,000 year period is 7.6×10^{-8} [40]. The free-water diffusivity of acrylonitrile is 1.66×10^{-5} cm/s at assumed down-hole conditions of temperature 110 °F (43.3 °C) and pressure 1100 psi (74.83 atm) [41].

Results and discussion

Subsurface flow

Figure 3 shows the 95% confidence limits on effective vertical permeabilities in the case of an isotropic two-dimensional formation with unit shale aspect ratio at various shale fractions. These confidence limits are based on a statistical analysis of the 600 simulations conducted at each shale fraction and indicate the sensitivity of the effective permeability to a particular subsurface configuration. In the case of high shale fractions, the flow path remains blocked for all sand–shale configurations. Conversely, at low shale fractions,

there is always a connecting sand flow path through the hypothetical confinement zone. At these two extremes of shale fraction, the uncertainty or variability in the effective vertical permeability is small and the effective permeability is independent of the particular configuration of the sand–shale formation. Since the blocking of flow paths depends on the particular configuration when the shale fraction is between about 0.5 and 0.6, the uncertainty or variability in the effective vertical permeability is largest in this case.

Estimates of effective vertical permeability in individual three-dimensional flow systems are also presented in Fig. 3. As the shale fraction of the confining layers increases, the number of iterations required for convergence in the predicted hydraulic head field increases due to flow blockage by the low permeability shale. Convergence is generally not obtained at high shale fractions unless the ratio of sand to shale permeability is much smaller [24]. In general, the effective vertical permeability for a three-dimensional flow system is within the range of uncertainty of the two-dimensional flow simulations. At low shale fraction there was little difference between the two dimensional and three dimensional simulations. At shale fractions above 0.70, shale blocking of

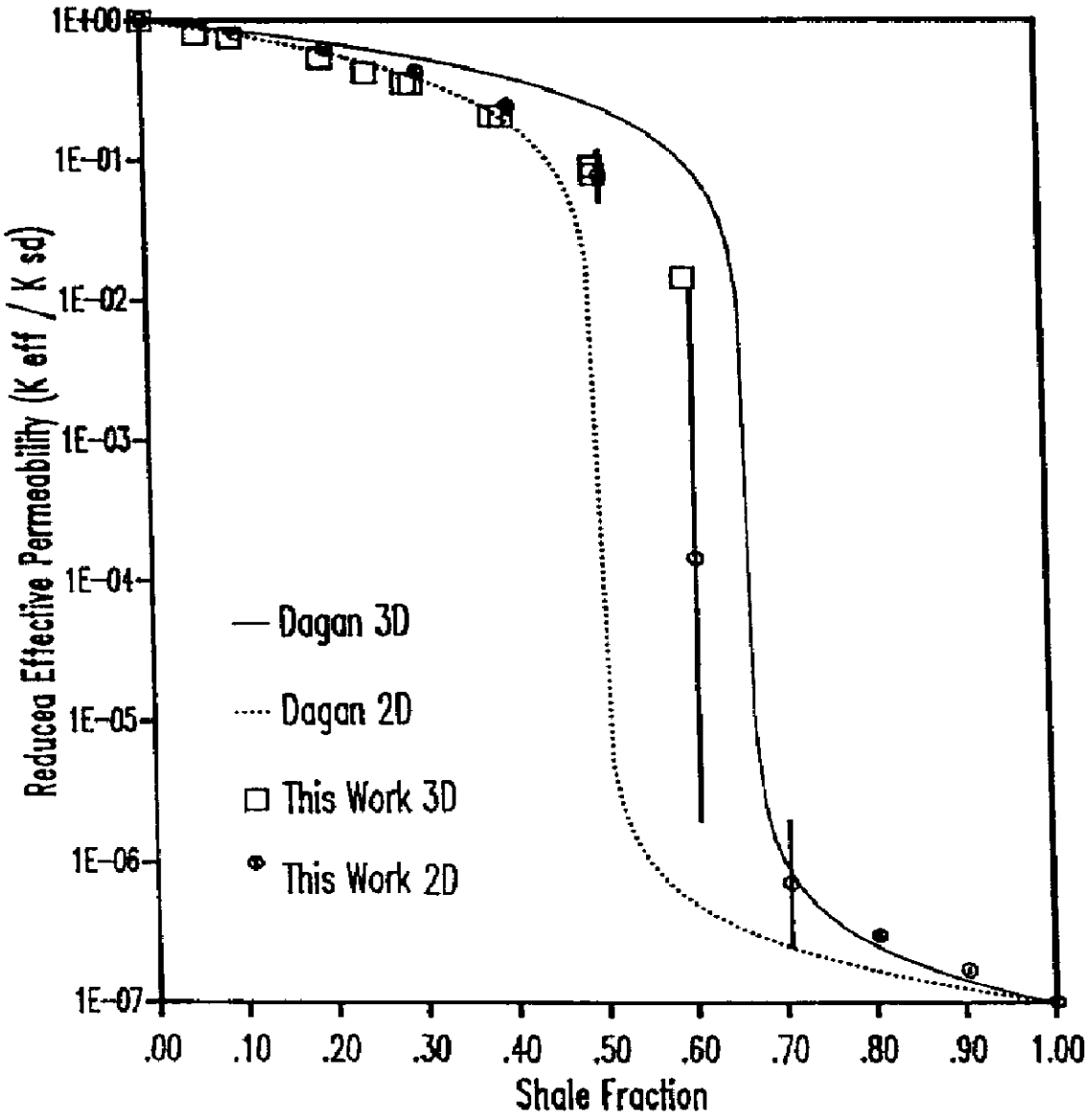

Fig. 3. Comparison of effective permeability between numerical results and Dagan's solutions. (Solid vertical lines associated with 2D numerical results represent 95% confidence limits.)

transport paths occurred and the effective permeability of the medium effectively approached that of pure shale. Only for intermediate shale fractions is there a potential effect of three dimensional versus two dimensional formation behavior.

This is also shown by examining the theoretical results of Dagan [13]. He employed the self-consistent approximation in which the media surrounding a certain element are treated as homogeneous with the global effective permeability. For the binary distribution and isotropic formation, the self-consistent formula of effective permeability from Dagan's paper reduces to

$$K_{\text{eff}} = \frac{1}{m}\left[\frac{F_{\text{sd}}}{(m-1)K_{\text{eff}} + K_{\text{sd}}} + \frac{F_{\text{sh}}}{(m-1)K_{\text{eff}} + K_{\text{sh}}}\right]^{-1}, \tag{8}$$

where K_{eff} is the effective permeability, K_{sh}, F_{sh} and K_{sd}, F_{sd} represent permeability and fraction of medium respectively for shale and sand, and m is 2 or 3 for two- and three-dimensional flows, respectively. In Fig. 3, the dotted line represents effective permeabilities for a two-dimensional flow system and the solid line represents effective permeabilities for a three-dimensional flow system. For $K_{\text{sd}} \gg K_{\text{eff}} \gg K_{\text{sh}}$ and $F_{\text{sd}} \sim F_{\text{sh}}$, Dagan's model suggests the effective permeability of a 3D system is much higher than that of a 2D system. Agreement between Dagan's analytical results and the simulations is satisfactory for shale fractions of less than about 0.5 or greater than 0.7.

Using information from a hazardous waste disposal well in Jefferson Parish, Louisiana as a field example, effective vertical permeabilities were calculated based on well log data. In this calculation, measured shale permeabilities were about 0.0005 mdarcy. The average shale fraction of the confining layer was 82%. Effective porosity was assumed to be 0.3. Isotropy was assumed to provide a higher than expected estimate of vertical migration. The mean vertical velocity of injected hazardous wastes was calculated from the expected value of the effective vertical permeability by using Darcy's law and the surface injection pressure as an upper bound to the actual driving pressure. The estimated mean vertical velocity was 0.03 cm/year. Over 10,000 years, therefore, the waste would be expected to penetrate only 3 m on average [27].

Contaminant transport

The maximum pressure difference across the confining layer was estimated by the injection pressure at 15.5 atm. As an upper bound to advective transport, waste injection and therefore injection pressure was assumed constant for the entire 10,000 years. If the injection of hazardous wastes was only continued for a finite time, the driving pressure would decrease and advective transport would result only from natural hydraulic head differences. Simulations assuming an injection period of less than 100 years yielded results after 10,000 years essentially identical to those assuming only diffusion was operative.

Desbarats [24] showed that vertical macrodispersive spreading is slightly greater in the stratified case than in the isotropic case. The effective vertical permeability and therefore the mean flow velocity, however, would decrease significantly as the aspect ratio increased, offsetting this effect [14, 27]. Hence, the choice of a shale aspect ratio of one provides an upper bound to flow and solute transport.

For steady-state flow and transient solute transport conditions, the two-dimensional Galerkin finite element method was applied to get individual concentrations in an isotropic formation. From the individual concentrations at each node, concentration isopleths were developed for the formations exhibiting shale fractions of 0.66, 0.7, 0.8 and 0.88. Concentration isopleths in the hypothetical confining layer were estimated at 10,000 years subject to both advection–dispersion and diffusion alone. The concentration isopleths for diffusion cases are represented in Figs. 4(a) and 5(a) and the concentration isopleths for advection–dispersion cases are shown in Figs. 4(b) and 5(b). The concentration isopleths generally matched the sand distribution in the configuration, that is, significant penetration of the confining layer was noted only where sand streaks existed. Schematic representations of hypothetical confining layers with different shale fractions have been described in Figs. 1 and 2.

The degree of horizontal non-uniformity of concentrations in the confining layer decreased as shale fraction increased. The degree of the non-uniformity of concentration also decreased as penetration of the confining layer increased. Over 10,000 years at a shale fraction of 0.66, the maximum vertical penetration of concentrations exceeding 0.1 (i.e 10% of injection concentration) by diffusion is 43 ft (13.11 m), while for advection–dispersion assuming a 10,000 year injection period is 61 ft (18.59 m). In these cases, the retardation factor was assumed to be unity in order to obtain the upper bound of vertical penetration. The difference in concentration between diffusion cases and advection–dispersion cases decreased as shale fraction was increased.

Mean concentration profile

The mean concentration profiles with depth were obtained for the diffusion case and advection–dispersion case using simple averaging along the width. As indicated above, the horizontal fluctuations from the mean decreased with depth into the confining layer. Figure 6 compares the mean concentration profiles for diffusion only with those for advection–dispersion at shale fraction 0.8. There is little difference in the mean concentration profiles before 1,000 years. At 10,000 years, however, the mean concentration results of advection–dispersion case are higher than those of the diffusion case. Since the vertical interstitial velocity was very small, solute transport was not affected by advection at shorter times. Results show the travel distance of acrylonitrile to a location where concentrations were 10 percent of that injected is about 41 ft (12.5 m).

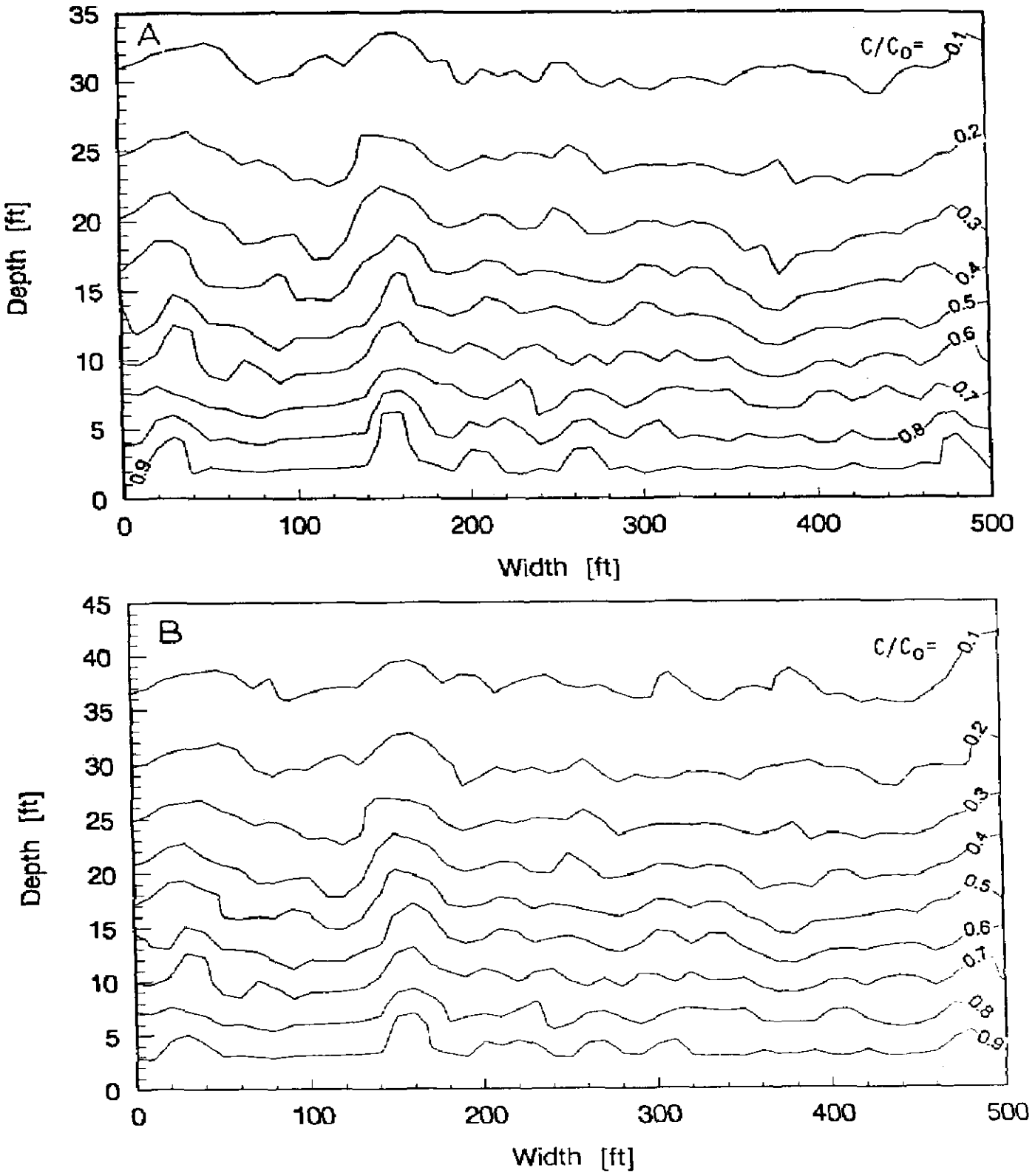

Fig. 4(A). Concentration isopleth for diffusion at shale fraction 0.66 after 10,000 years. (B) Concentration isopleth for advection–dispersion at shale fraction 0.66 after 10,000 years.

In order to investigate the effect of sorption related retardation on transport in confining layers, partition coefficients of 0, 0.25, 0.5, 1, and 3 were used in the advection–dispersion equation. In this case, the shale fraction was 0.66. Since there was little interaction between hazardous wastes and sand, a partition coefficient was only applied to the shale regions. In shale zones, the bulk density of the solid phase and the porosity in shale were assumed to be 1.67 and 0.3, respectively. The retardation factor was changed from 1 to 17.7 as a result of the variation of the partition coefficient between 0 and 3. Figure 7 illustrates the effect of partition coefficients on the mean concentration profile after 10,000 years. The travel distance in the direction of mean flow at dimensionless concentration 0.5 is inversely proportional to $\sqrt{R_f}$. Even though the retardation factor was only applied to randomly placed shale zones, the trend of this

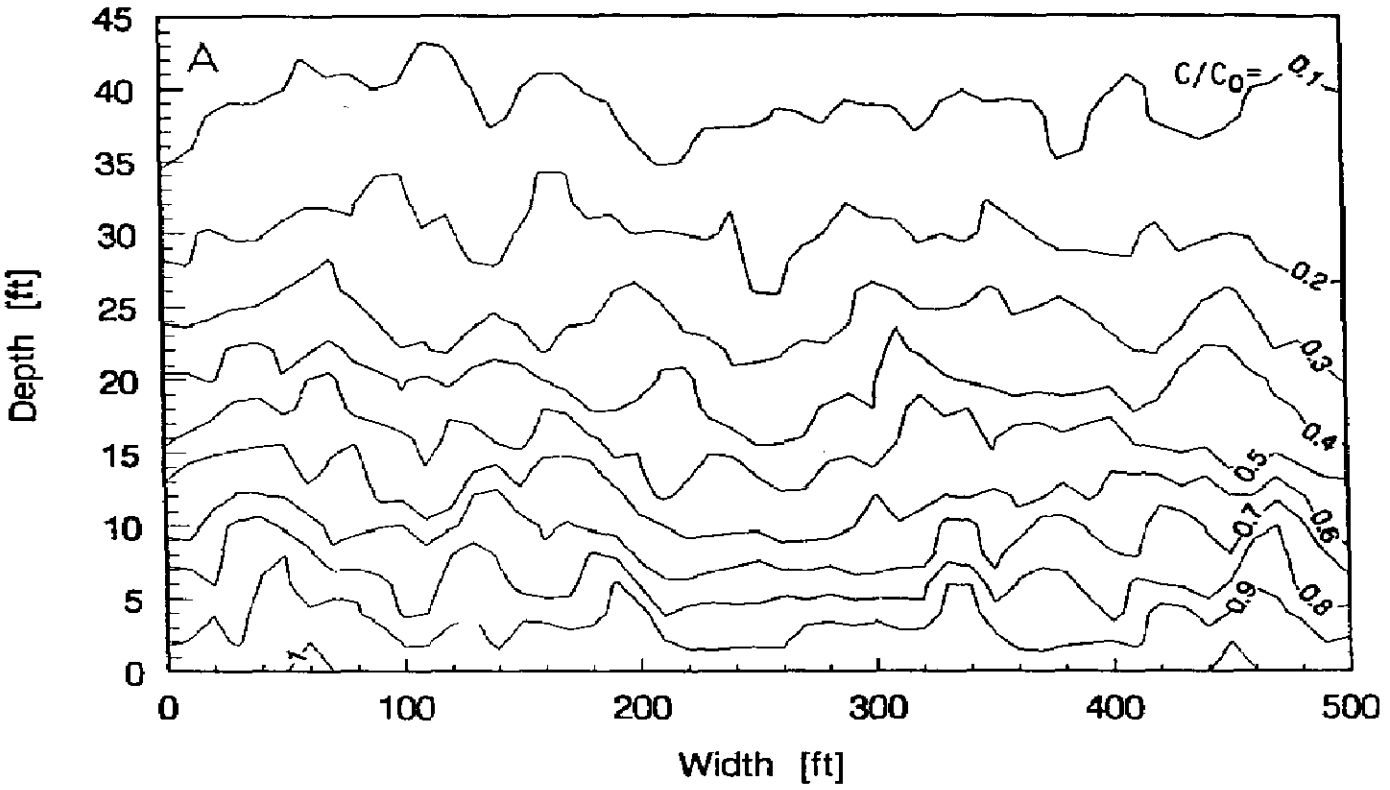

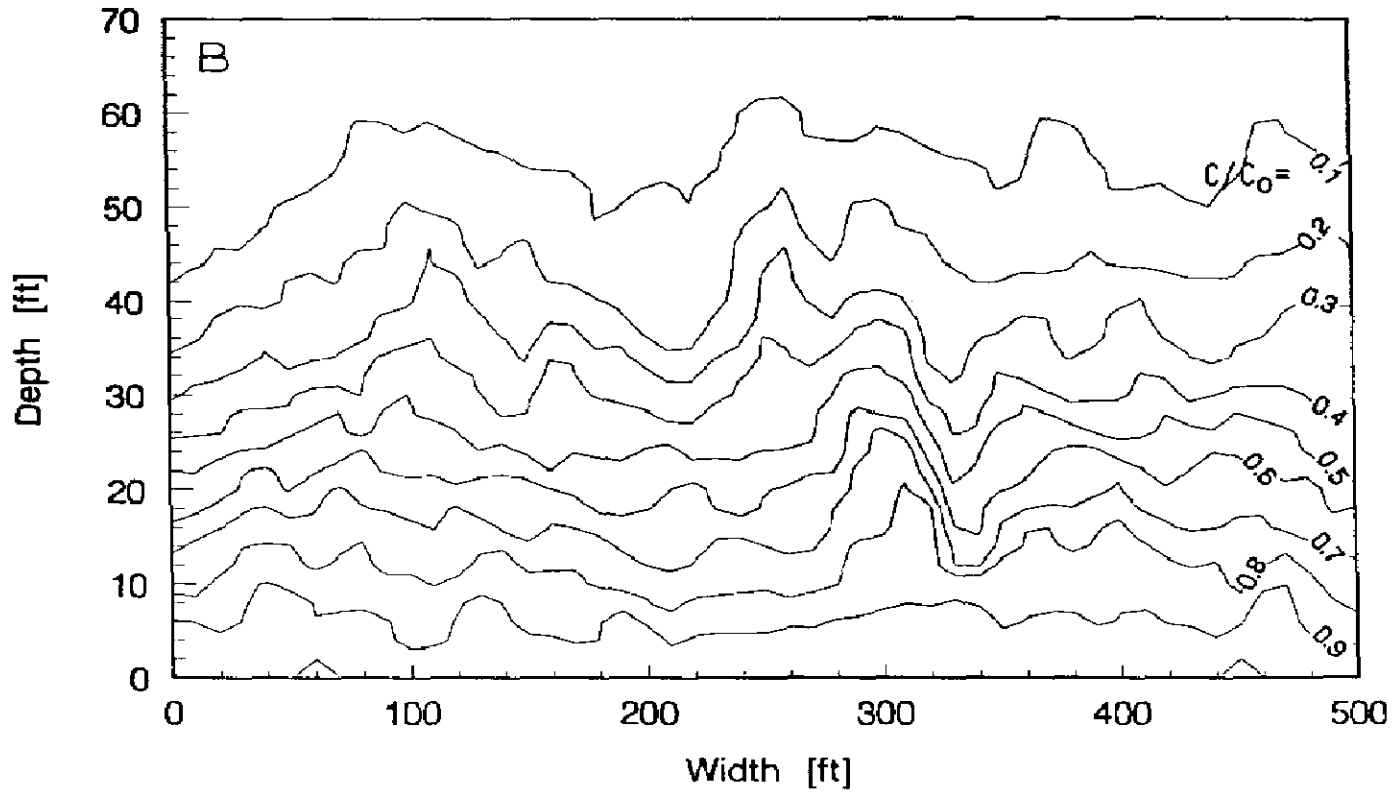

Fig. 5(A). Concentration isopleth for diffusion at shale fraction 0.88 after 10,000 years. (B) Concentration isopleth for advection–dispersion at shale fraction 0.88 after 10,000 years.

result is identical to that expected for pure shale formations. Hence, the model again illustrates that solute transport through the sand–shale formation was dominated by the hydrodynamic properties of shale regions in higher shale fractions.

Penetration depth

To insure containment of the injected wastes, it is desired to estimate the depth of penetration of concentrations exceeding drinking water standards. The distance to achieve a given dilution ratio for various shale fractions is shown in Fig. 8. The required dilution ratio to achieve drinking water standards for acrylonitrile is 7.6×10^{-8} in the example waste stream. Table 1 presents the mean penetration depth based on meeting the required dilution for

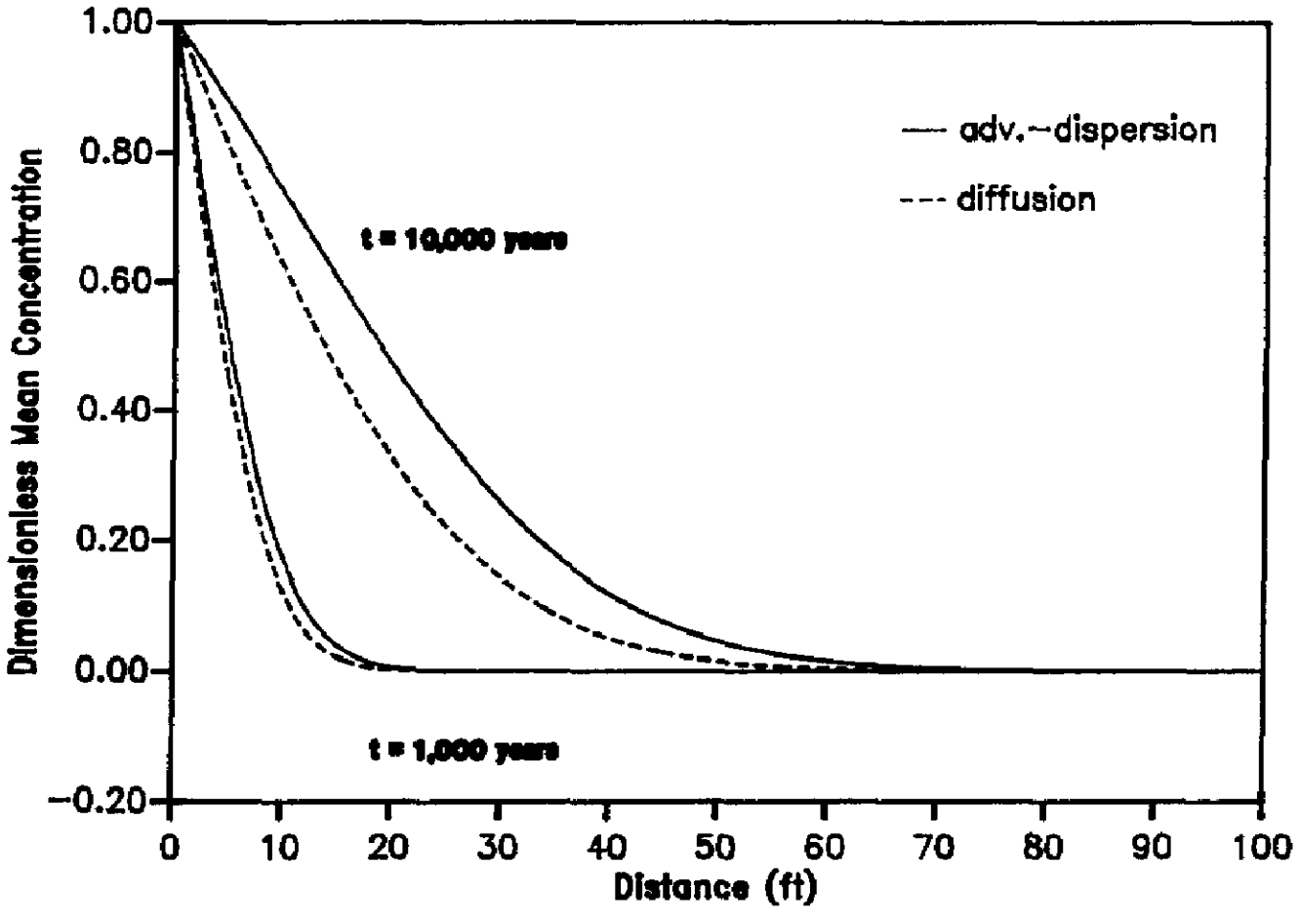

Fig. 6. Comparison of mean concentration between diffusion and advection–dispersion with time at shale fraction 0.8.

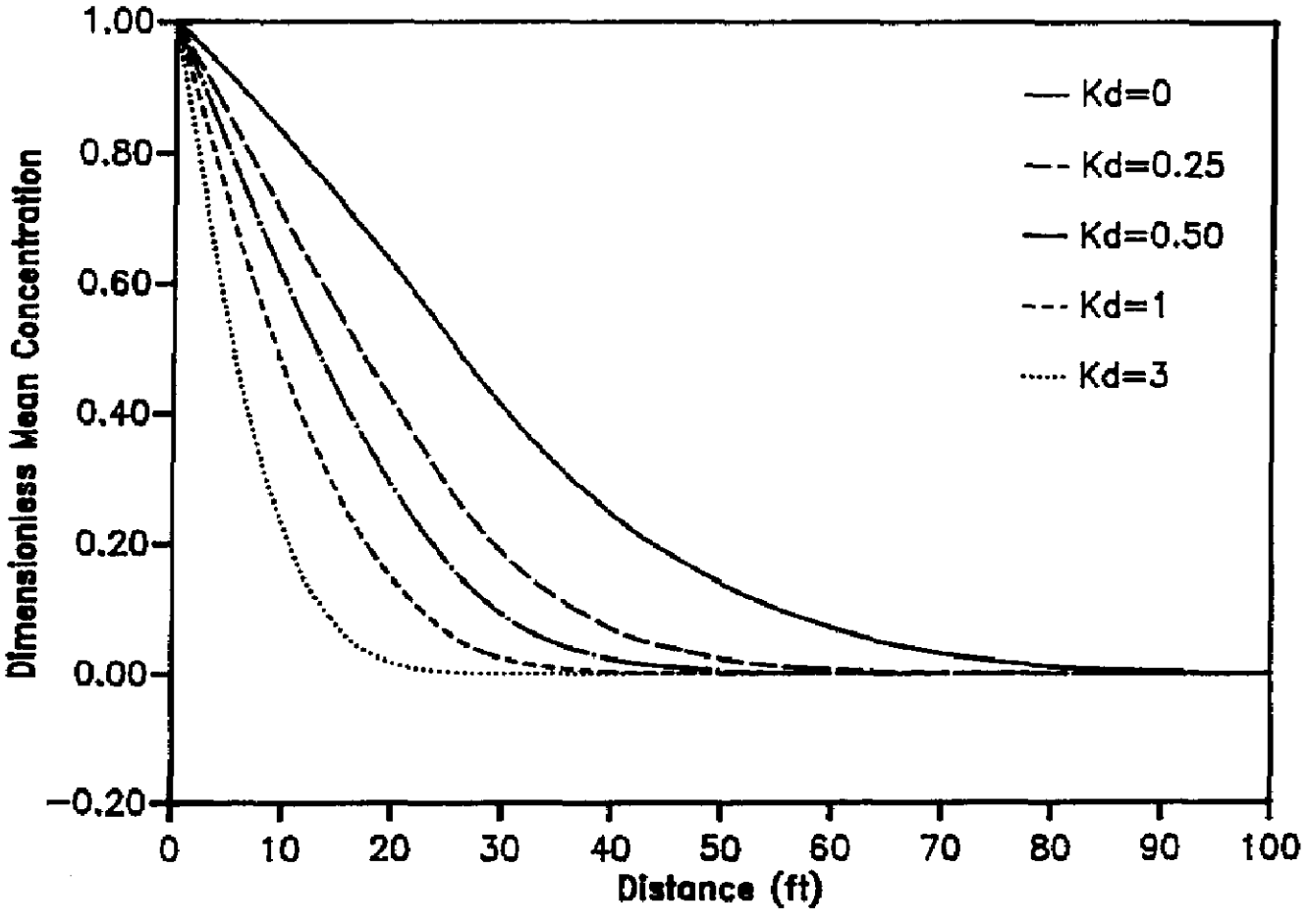

Fig. 7. Effect of partition coefficient to mean concentration at shale fraction 0.66 after 10,000 years.

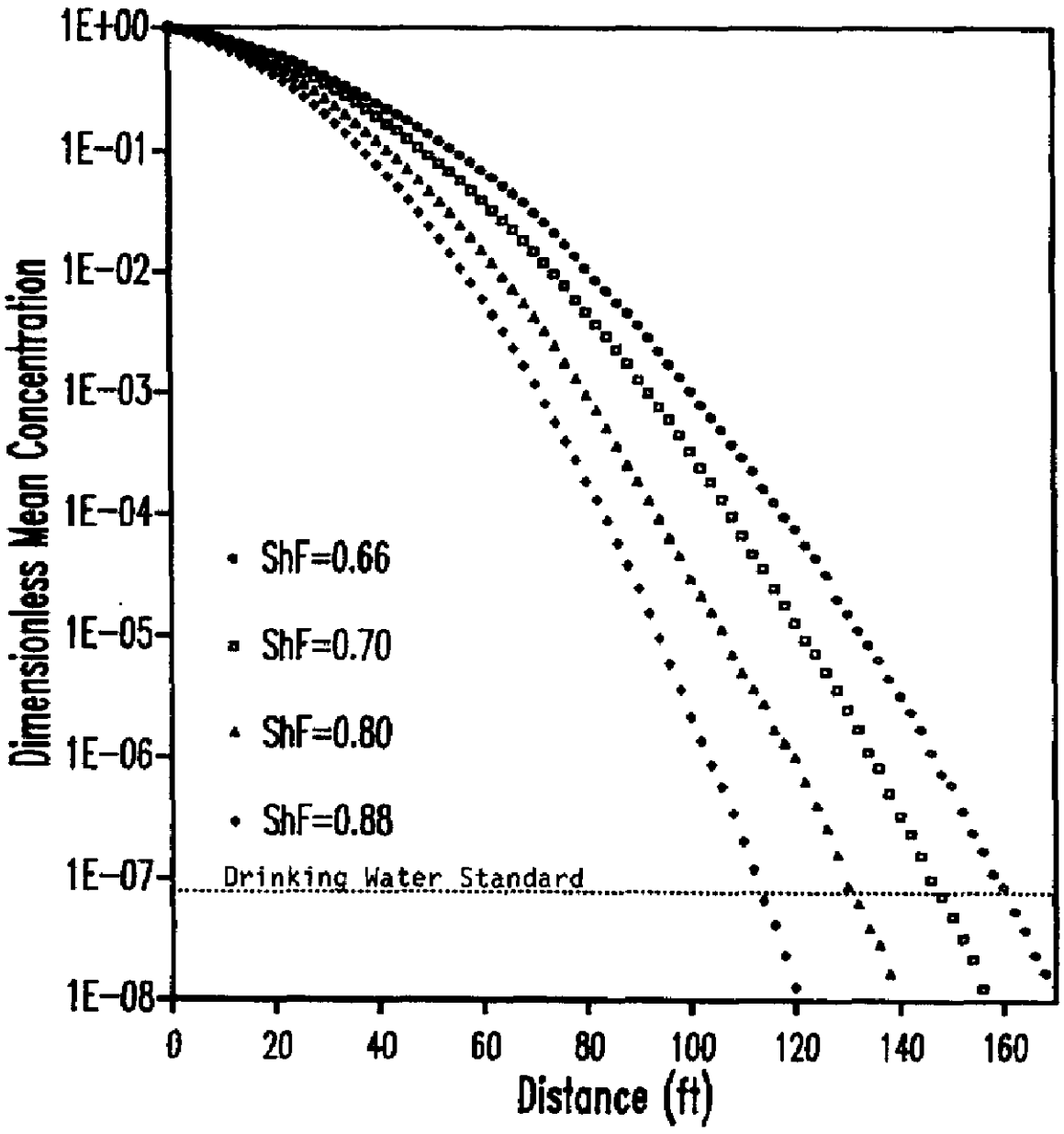

Fig. 8. Mean concentration profiles for advection–dispersion with shale fraction after 10,000 years.

TABLE 1

Mean penetration depth for advection–dispersion and diffusion with the change of shale fraction in 10,000 years

Shale fraction	Mean penetration depth (m)	
	Advection–dispersion[a]	Diffusion
0.66	48.4	38.9
0.70	44.6	37.7
0.80	38.8	33.9
0.88	34.6	31.0

[a] Injection for entire 10,000 year period.

both diffusion and advection–dispersion after 10,000 years. The mean penetration depth was inversely proportional to the shale fraction in both advection–dispersion and diffusion. Lateral variability led to deeper penetration in some areas than in others. Table 2 shows the equivalent maximum penetration depths based on the mean concentration profiles plus two standard deviations.

TABLE 2

Maximum penetration depth for advection–dispersion and diffusion with the change of shale fraction 10,000 years

Shale fraction	Maximum penetration depth (m)	
	Advection–dispersion[a]	Diffusion
0.66	53.0	42.5
0.70	48.5	41.0
0.80	44.0	37.6
0.88	37.1	33.0

[a] Injection for entire 10,000 year period.

The maximum penetration depth for advection–dispersion after 10,000 years is less than 200 ft (60.96 m).

The simulation suggests that the injected hazardous wastes will be confined in the disposal zone for the EPA required 10,000 years. This analysis does not consider, however, the effect of loss of integrity of the injection well resulting in injection outside of the confining layer or the effect of non-random artificial penetrations of the confining layers such as unsealed inactive oil production wells. In addition, estimates with a lower than 50% shale fraction confining layer suggested that deep-well injection in such a geology could result in waste penetration of the 200 ft confining layer within 500 years if the injection pressure were maintained throughout. These results are also dependent on the accuracy of the estimated diffusion coefficient. An error by an order of magnitude in effective diffusion coefficient would change the effective penetration depth by diffusion alone by a factor of three.

Summary and conclusions

Hypothetical confining layers were modeled as a combination of binary random structures composed of either pure sand or pure shale. Monte Carlo techniques were used to generate the configuration of confining layers. Flow and solute transport assuming a constant pressure driving force over 10,000 years, 100 years and with diffusion alone were investigated by using the Galerkin finite element method for four hypothetical configurations with shasle fractions of 0.66, 0.7, 0.8, and 0.88.

At low shale fractions, less than 0.4, the effective permeability of the formation was essentially that of pure sand. At high shale fractions, greater than 0.65–0.7, the effective permeability of the formation was essentially that of pure shale. At either of these extremes, the effective permeability and the average flow and transport behavior was insensitive to the particular sub-surface configuration. Two- and three-dimensional estimates of effective

permeability of the subsurface formation are also similar at low shale fraction.

Transport modeling showed deeper penetration of deep-well injected contaminants in local sand veins. Since sand veins were not continuous throughout the modeled confining layer at high shale fractions, the maximum penetration was still small for the confining layer structures considered. The degree of horizontal non-uniformity of concentrations decreased as shale fraction or depth into confining layer increased.

Comparison between an advection–dispersion model and a diffusion only model showed differences that increased with time. These differences decreased as shale fraction increased because advection decreased with increasing shale fraction. Sorption in the heterogeneous confining layer significantly retarded the movement of a compound, despite the assumption that only limited sorption occurred primarily in shale zones.

In a particular injected waste and subsurface geology, the mean and the maximum penetration depths of waste water containing acrylonitrile concentrations in excess of drinking water standards over 10,000 years were less than 200 ft (60.96 m). These penetration depths were less than the thickness of the confining layers, which were usually greater than 300 ft (91.44 m).

Acknowledgment

This research was supported in part by members of the Louisiana Chemical Association in an unrestricted grant through the Hazardous Waste Research Center and the LSU Foundation at Louisiana State University.

References

1 W. Gordon and J. Bloom, Limits to underground injection as a hazardous waste disposal method, Hazard. Waste Hazard. Mater., 2(4) (1985) 411–451.
2 Federal Register, 40 CFR 124, 144, 148, 52(166), Washington, DC, August, 1987.
3 G.E. Fogg, Groundwater flow and sand body interconnectedness in a thick, multiple-aquifer system, Water Resour. Res., 22(5) (1986) 679–694.
4 S.E. Silliman and A.L. Wright, Stochastic analysis of paths of high hydraulic conductivity in porous media, Water Resour. Res., 24(11) (1988) 1901–1910.
5 L. Smith and R.A. Freeze, Stochastic analysis of steady state groundwater flow in a bounded domain. 1. One-dimensional simulation, Water Resour. Res., 15(6) (1979) 521–528.
6 L. Smith and R.A. Freeze, Stochastic analysis of steady state groundwater flow in a bounded domain. 2. Two-dimensional simulation, Water Resour. Res., 15(6) (1979) 1543–1559.
7 J.E. Warren and H.S. Price, Flow in heterogeneous porous media, Soc. Pet. Eng. J., 1 (1961) 153–169.
8 A.A. Bakr, L.W. Gelhar, A.L. Gutjahr and J.R. McMillan, Stochastic analysis of spatial variability in subsurface flow. 1. Comparison of one- and three-dimensional flows, Water Resour. Res., 14(2) (1978) 263–271.

9 A.L. Gutjahr, L.W. Gelhar, A.A. Bakr and J.R. McMillan, Stochastic analysis of spatial variability in subsurface flow. 2. Evaluation and application, Water Resour. Res., 14(5) (1978) 953–959.
10 L.W. Gelhar and C.L. Axness, Three-dimensional stochastic analysis of macrodispersion in aquifers, Water Resour. Res., 19(1) (1983) 161–180.
11 G. Matheron, Composition des permeabilities en milieu poreux hétérogène: Méthode de Schwydler et règles de ponderation, Rev. Inst. Fr. Pet., 22 (1967) 443–466.
12 A.J. Desbarats, Numerical estimation of effective permeability in sand-shale formations, Water Resour. Res., 23(2) (1987) 273–286.
13 G. Dagan, Models of groundwater flow in statistically homogeneous porous formations, Water Resour. Res., 15(1) (1979) 47–63.
14 J.W. Kramers, S. Bachu, D.L. Cuthiell, M.E. Prentice and L.P. Yuan, A multidisciplinary approach to reservoir characterization: the Provost upper Mannville B pool, J. Can. Pet. Technol., 28(3) (1989) 1–11.
15 H.H. Haldorsen and L.W. Lake, A new approach to shale management in field scale methods, Soc. Pet. Eng. J., August (1984) 447–457.
16 S.H. Begg, D.M. Chang and H.H. Haldorsen, A simple statistical method of calculating the effective vertical permeability of a reservoir containing discontinuous shales, In: Proc. 60th Annu. Tech. Conf., Soc. of Pet. Eng., Las Vegas, NV, Sept. 1985 pp. 22–25.
17 L.W. Gelhar, A.L. Gutjahr and R.L. Naff, Stochastic analysis of macrodispersion in a stratified aquifer, Water Resour. Res., 15(6) (1979) 1387–1397.
18 J.F. Pickens and G.E. Grisak, Scale-dependent dispersion in a stratified granular aquifer, Water Resour. Res., 17(4) (1981) 1191–1211.
19 G. Dagan, Time-dependent macrodispersion for solute transport in anisotropic heterogeneous aquifers, Water Resour. Res., 24(9) (1988) 1491–1500.
20 G. Dagan, Solute transport in heterogeneous porous formations, J. Fluid Mech., 145 (1984) 151–177.
21 G. Dagan, Statistical theory of groundwater flow and transport: Pore to laboratory, laboratory to formation, and formation to regional scale, Water Resour. Res., 22(9) (1986) 120s–134s.
22 S.P. Neuman, C.L. Winter and C.M. Newman, Stochastic theory of field-scale Fickian dispersion in anisotropic porous media, Water Resour. Res., 23(3) (1987) 453–466.
23 A.F.B. Tompson and L.W. Gelhar, Numerical simulation of solute transport in three-dimensional, randomly heterogeneous porous media, Water Resour. Res., 26(10) (1990) 2541–2562.
24 A.J. Desbarats, Macrodispersion in sand–shale sequences, Water Resour. Res., 26(1) (1990) 153–163.
25 G. Segol, G.F. Pinder and W.G. Gray, A Galerkin-finite element technique for calculating the transient position of the saltwater front, Water Resour. Res., 11(2) (1975) 343–347.
26 W.E. Galloway, D.K. Hobday and K. Magara, Frio formation of the Texas Gulf Coast Basin — Depositional systems, structural framework, and hydrocarbon origin, migration, distribution, and exploration potential, Report of Investigations No. 122, University of Texas at Austin, Bureau of Economic Geology, Austin, TX, 1982, p. 78.
27 S.W. Rhee, D.D. Reible and W.D. Constant, Simulation of the effects of shale heterogeneities on effective permeability in deep-well injection disposal systems, Fluid/Particle Sep. J., 4(4) (1991) 204–210.
28 R.A. Freeze and J.A. Cherry, Groundwater, Prentice-Hall, Englewood Cliffs, NJ, 1979.
29 W.D. Constant and D.A. Clark, Experimental evaluation of containment properties for shale associated with deep-well hazardous waste injection zone, Proc. 6th Conf. and Exhibition on Hazardous Waste and Hazardous Material, New Orleans, LA, April 1989, pp. 182–187.

30 M.G. McDonald and A.W. Harbaugh, A modular three-dimensional finite difference ground-water flow model, U.S. Geological Survey, Ruston, VA, 1988.
31 J. Bear, Dynamics of Fluids in Porous Media, Elsevier, New York, 1972.
32 I.M. Smith and D.V. Griffiths, Programming the Finite Element Method, 2edn., Wiley, New York, 1988.
33 S.P. Neuman, Universal scaling of hydraulic conductivities and dispersivities in geologic media, Water Resour. Res., 26(8) (1990) 1749–1758.
34 R.J. Millington and J.P. Quirk, Permeability of porous solids, Trans. Faraday Soc., 57 (1961) 1200–1207.
35 R.A. Berner, Early Diagenesis: A Theoretical Approach, Princeton University Press, Princeton, NJ, 1980.
36 V. Ranganathan and J.S. Hanor, Density-driven groundwater flow near salt domes, Chem. Geol., 74 (1988) 173–188.
37 S.W. Karickhoff, D.S. Brown and T.A. Scott, Sorption of hydrophobic pollutants on natural sediments, Water Res., 13 (1979) 241–248.
38 W.J. Green, G.F. Lee, R.A. Jones and T. Pallt, Interaction of clay soils with water and organic solvents: Implications for the disposal of hazardous wastes, Environ. Sci. Technol., 17 (1983) 278–282.
39 U.S. EPA., Superfund public health evaluation manual. Draft. Prepared by ICF, Inc. for the Policy Analysis Staff, Office of Emergency and Remedial Response, Washington, DC. U.S. Environmental Protection Agency, October 1, 1985.
40 INTERA Technologies, Inc., Mathematical modeling for the American Cyanamid Fortier Facility, Austin, TX, 1988.
41 W. Hayduk and H. Laudie, Prediction of diffusion coefficients for nonelectrolytes in dilute aqueous solutions, AIChE J., 20 (1974) 611–615.